Journal of Biomedical Optics

SPIEDigitalLibrary.org/jbo

Real-time *in vivo* Cherenkoscopy imaging during external beam radiation therapy

Rongxiao Zhang
David J. Gladstone
Lesley A. Jarvis
Rendall R. Strawbridge
P. Jack Hoopes
Oscar D. Friedman
Adam K. Glaser
Brian W. Pogue

SPIE

Real-time *in vivo* Cherenkoscopy imaging during external beam radiation therapy

Rongxiao Zhang,[a,d] David J. Gladstone,[b,c] Lesley A. Jarvis,[b,c] Rendall R. Strawbridge,[e] P. Jack Hoopes,[e] Oscar D. Friedman,[a] Adam K. Glaser,[d] and Brian W. Pogue[a,b,d,e]
[a]Dartmouth College, Department of Physics and Astronomy, Hanover, New Hampshire 03755
[b]Dartmouth-Hitchcock Medical Center, Norris Cotton Cancer Center, Lebanon, New Hampshire 03766
[c]Dartmouth College, Geisel School of Medicine, Department of Medicine, Hanover, New Hampshire 03755
[d]Dartmouth College, Thayer School of Engineering, Hanover, New Hampshire 03755
[e]Geisel School of Medicine at Dartmouth, Department of Surgery, Hanover, New Hampshire 03755

Abstract. Cherenkov radiation is induced when charged particles travel through dielectric media (such as biological tissue) faster than the speed of light through that medium. Detection of this radiation or excited luminescence during megavoltage external beam radiotherapy (EBRT) can allow emergence of a new approach to superficial dose estimation, functional imaging, and quality assurance for radiation therapy dosimetry. In this letter, the first *in vivo* Cherenkov images of a real-time Cherenkoscopy during EBRT are presented. The imaging system consisted of a time-gated intensified charge coupled device (ICCD) coupled with a commercial lens. The ICCD was synchronized to the linear accelerator to detect Cherenkov photons only during the 3.25-μs radiation bursts. Images of a tissue phantom under irradiation show that the intensity of Cherenkov emission is directly proportional to radiation dose, and images can be acquired at 4.7 frames/s with SNR > 30. Cherenkoscopy was obtained from the superficial regions of a canine oral tumor during planned, Institutional Animal Care and Use Committee approved, conventional (therapeutically appropriate) EBRT irradiation. Coregistration between photography and Cherenkoscopy validated that Cherenkov photons were detected from the planned treatment region. Real-time images correctly monitored the beam field changes corresponding to the planned dynamic wedge movement, with accurate extent of overall beam field, and expected cold and hot regions. [DOI: 10.1117/1.JBO.18.11.110504]

Keywords: Cerenkov; Cherenkov; dosimetry; dose; radiation therapy; linear accelerator; Cherenkoscopy.

Address all correspondence to: Brian W. Pogue, Dartmouth College, Department of Physics and Astronomy, Hanover, New Hampshire 03755. Tel: 1-603-646-3861; Fax: 1-603-646-3856; E-mail: Brian.W.Pogue@dartmouth.edu or Rongxiao Zhang, Dartmouth College, Department of Physics and Astronomy, Hanover, New Hampshire 03755. Tel: 1-603-646-6506; Fax: 1-603-646-3856; E-mail: Rongxiao.Zhang.GR@dartmouth.edu

Paper 130679LR received Sep. 17, 2013; revised manuscript received Oct. 12, 2013; accepted for publication Oct. 15, 2013; published online Nov. 18, 2013.

Cherenkov radiation emission occurs in all dielectric media (such as water and biological tissue) when charged particles move with phase velocity greater than the speed of light in that medium.[1] This Cherenkov effect produces a broad spectrum of light emission from UV down to near-infrared, with a spectrum described by the Frank-Tamm formula, varying as the inverse square of wavelength.[2] Recent work has shown, in phantoms, small animals,[3] and clinical patients,[4] that Cherenkov emission is generated by $\beta+$ and $\beta-$ emitters in diagnostic (18-FDG) and nuclear medicine (131-I) applications. However, to date, Cherenkov radiation emission has never been imaged *in vivo* during external beam radiation therapy (EBRT), where there is considerable signal throughout the treated regions of tissue. In this letter, we present the first linearity test between surface dose and Cherenkov emission in a phantom, followed by the first video sequence of Cherenkov emission *in vivo*. This imaging is here named Cherenkoscopy, for the parallel between fluoroscopy but with surface imaging of Cherenkov signal. The imaging was performed while a dog was undergoing planned EBRT for treatment of a spontaneous oral tumor.

The occurrence of Cherenkov radiation in water during megavoltage EBRT with both electron and photon beams has been demonstrated in several recent papers.[5,6] Based on the detection of Cherenkov radiation or excited luminescence during EBRT, techniques such as radiation beam profiling,[6–8] oximetry,[9,10] and superficial radiation dosimetry have been investigated in phantoms.[11,12] While the utility of this emission is still under investigation, the applications are likely dependent on the ease of imaging and the frame rate of acquisition. In this study, the goal was to assess the feasible frame rate for imaging emission from tissue and confirm that there would be sufficient signal to noise for near real-time imaging.

The experimental configuration is shown in Fig. 1(a). The external beam irradiator was a Varian Clinic 2100CD linear accelerator (LINAC, Varian Medical Systems, Palo Alto, CA). A time-gated intensified charge coupled device (ICCD) camera was set up on a tripod to image the entrance region of the treatment beam on tissue phantoms or tissue. The LINAC delivers radiation in pulsed mode, as described in Fig. 1(b), and the ICCD camera was synchronized to the 3-μs radiation bursts, detecting Cherenkov emission effectively and rejecting most of the ambient light.[13] This imaging system was first tested by imaging Cherenkov emission from a slab ($30 \times 30 \times 4$ cm^3) phantom made of opaque water equivalent plastic while irradiating it with a 6 MV square (10×10 cm^2) photon beam at a dose rate of 600 monitor units (MU, 1 MU = 1 cGy for 10×10 cm^2 field at $d_{\max}$) per minute. Cherenkov images for different delivered doses at $d_{\max}$ (0.5 to 25 cGy) were acquired.

After background subtraction, the Cherenkov images of the flat phantom for dose at $d_{\max}$ from 0.5 to 25 cGy (corresponding to fps from 7 to 0.68) are shown in Fig. 2(a). It has been shown by Archambault et al.,[14] for CCD cameras, that median filtering is an effective method for sparkle noise removing. To remove the sparkle noisy pixels caused by high-energy photon hitting the ICCD directly, each image was generated by median filtering over a stack of three images from repetitive measurements and then smoothed by a median filter with kernel size of 10 pixels × 10 pixels. The signal-to-noise ratio (SNR) of images acquired with different frame rates from 0.68 to 7

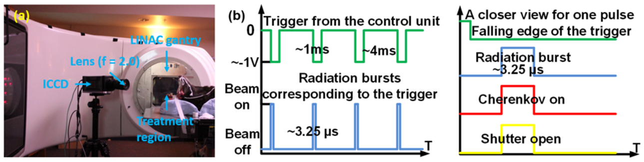

Fig. 1 (a) Relative positions of the linear accelerator (LINAC) gantry, treatment region, and the time-domain gated system. The intensified charge coupled device (ICCD) was synchronized to radiation bursts from the LINAC and Cherenkoscopy were taken from the beam incident on the treatment regions. (b) Timeline about the temporal gating.

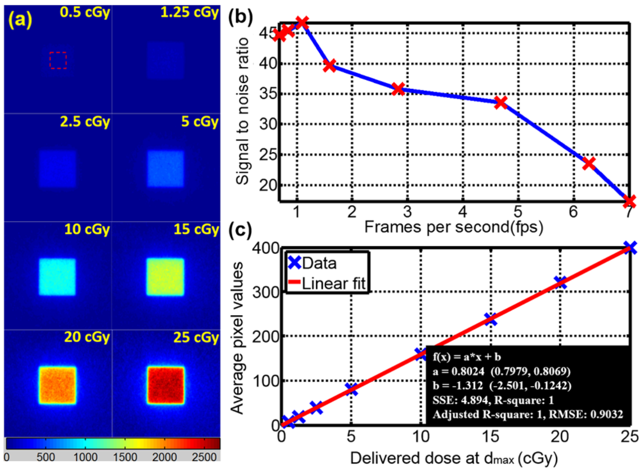

Fig. 2 (a) Cherenkoscopy from a 6 MV square (10×10 cm^2) photon beam incident normally on a tissue phantom ($30 \times 30 \times 4$ cm^3) of opaque water equivalent phantom at SSD $= 100$ cm with delivered dose at $d_{\max}$ varying from 0.5 to 25 cGy. (b) Signal-to-noise ratio of Cherenkov images with fps from 0.68 to 7. (c) Linearity between intensity of Cherenkov emission from the surface and delivered dose is established under these controlled conditions.

were calculated (mean value over the standard deviation) based on a chosen region (100 pixels $\times$ 100 pixels around the center) as indicated by a dotted red box in Fig. 2(a). SNR values were plotted with the corresponding frame rates in Fig. 2(b). To ensure relatively good image quality as well as real-time data acquisition, an accumulation of 50 radiation bursts (fps $= 4.7$) for each image was chosen as the imaging procedure for the following *in vivo* imaging. The average pixel value of each image was calculated and plotted with the corresponding delivered dose in Fig. 2(c). Least square linear fitting was applied and the results of the fitting are listed in Fig. 2(c). The good linearity ($R^2 = 1$) between Cherenkov intensity and delivered dose suggests that Cherenkoscopy could be a novel technique for superficial dose estimation. Our previous work focusing on a phantom study validated that, in tissue equivalent phantom, Cherenkov emission could sample superficial dose up to 6 mm and could be taken as surrogate of radiation dose in the sampling region with average discrepancy of 1%.[11,12] Within the scope of this short note, we focus on validating the fast imaging capabilities of Cherenkoscopy *in vivo* and correlate this signal to superficial dose qualitatively within the process of EBRT.

As shown in Fig. 3(a), a treatment plan was designed in Eclipse independently to treat a dog with a spontaneous oral tumor without considering the process of Cherenkoscopy. The LINAC was set to irradiate the treatment region with 6 MV photon beam, at a dose rate of 600 MU/ min. A total dose of 59 MU (reference dose of 60.5 cGy) was delivered. A dynamic wedge [indicated in Fig. 3(a)] was designed to control the beam dynamically during the treatment, delivering a homogenous dose distribution even in the presence of complex tissue geometry. Detailed information about the treatment field and the dynamic wedge are listed in Table 1. In order to deliver radiation dose to the tumor, high-energy radiation has to incident on the surface externally and results in certain amount of radiation dose to be deposited near the surface. The deposited dose near the surface of the treatment region was predicted by Eclipse and shown in Fig. 3(a). Since phantom studies validated that image quality (SNR > 30) and fast imaging capability (fps $= 4.7$) are balanced by an accumulation of 50 radiation bursts, Cherenkoscopy was acquired using this acquisition procedure. The tungsten light in the radiotherapy room was turned on to provide a reasonable level of ambient light while imaging. The background image was acquired with the same procedure before the treatment (radiation off), and background subtraction was applied simultaneously during the process of data acquisition. Figure 3(b) shows the photographic view of the

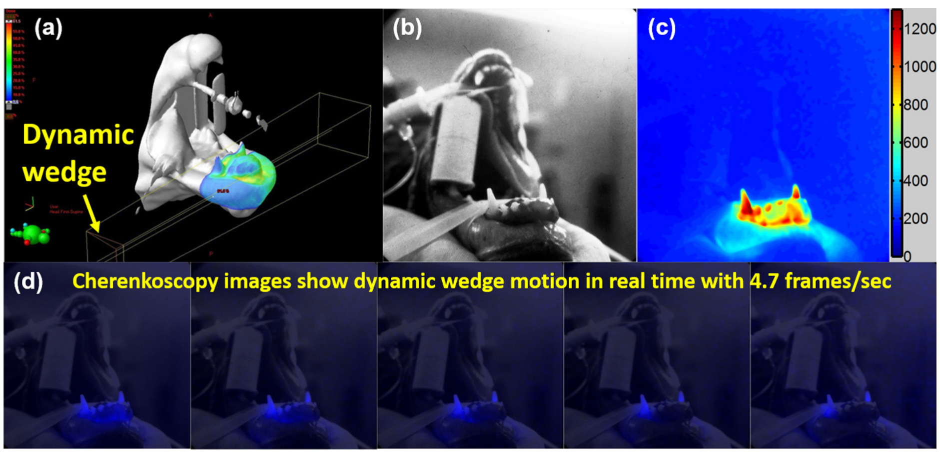

Fig. 3 (a) The treatment plan shows incident of the beam and dynamic wedge. Surface dose was calculated by the treatment planning system (Eclipse) and mapped on the surface of the treatment region. (b) Field view of the treatment region from the gated ICCD system. (c) Cherenkoscopy of the treatment region while irradiation progresses. (d) Cherenkoscopy overlaid on the white-light images of the treatment field and sequence of Cherenkoscopy showing the beam field changing while a wedge is moved into the beam to shape the integrated dose on the field. (Video 1, MOV, 19.5 MB) [URL: http://dx.doi.org/10.1117/1.JBO.18.11.110504.1].

Table 1 Parameters of the treatment plan.

Technique	Machine/energy	Gantry (deg)	Collimator (deg)	Couch (deg)	Wedge
STATIC-I	CD 120 - 6X	90.0	180.0	180.0	EDW20OUT
Field X (cm)	X1 (cm)	X2 (cm)	Field Y (cm)	Y1 (cm)	Y2 (cm)
5.4	+3.5	+1.9	5.9	+1.6	+4.2
X (cm)	Y (cm)	Z (cm)	SSD (cm)	Monitor units	Ref. dose (cGy)
−2.48	−1.52	−1.26	95.0	59	60.5

entrance region from the imaging system. The colorized *in vivo* Cherenkoscopy [Fig. 3(c)] corresponding to the treatment plan described in Fig. 3(a) and Table 1 was generated by averaging all the frames of images taken during the treatment and smoothed by a median filter with kernel size of 10 pixels× 10 pixels. In the first image of Fig. 3(d), Cherenkoscopy was coregistered to the photographic view by adding the Cherenkoscopy to the blue channel. It can be validated that the detected Cherenkov emission is from the treatment region. To the extent of overall beam field shape, hot and cold regions, the Cherenkoscopy [Fig. 3(c)] shows similar distribution compared with the predicted surface dose [Fig. 3(a)]. The hot regions in Cherenkoscopy around the teeth disagree with the predicted dose due to the relatively low absorption of Cherenkov photons by the teeth. Figure 3(d) shows frames of coregistered Cherenkoscopy monitored throughout the entire treatment. To remove the noise caused by high-energy photons hitting the ICCD directly, images were processed by median filtering over a stack of images including the two adjacent frames and then smoothed by a median filter with kernel size of 10 pixels × 10 pixels. Beam changes corresponding to the planned dynamic wedge were monitored by Cherenkoscopy in real time (fps = 4.7). A video (Video 1) of Cherenkoscopy of this treatment was produced with processed frames. Video 1 shows the monitoring of the entire treatment based on Cherenkoscopy, including the field changes due to the dynamic wedge movement at the end of the video.

In this study, we demonstrated that the concept of *in vivo* Cherenkoscopy is feasible in real time during EBRT, with acceptable SNR. It has been shown that Cherenkov emission is directly proportional to the delivered radiation surface dose in a tissue equivalent phantom [Fig. 2(c)]. The relatively low absorption of Cherenkov photons in the teeth lead to hot regions in Cherenkoscopy and a disagreement with the predicted surface dose. However, in the regions where the optical properties are relatively homogenous, Cherenkoscopy [Fig. 3(c)] shows similar hot and cold regions as compared to the predicted surface dose [Fig. 3(a)]. The next stage of evaluation of this technology will be *in vivo* Cherenkoscopy of human patients to monitor treatments, correlate superficial dose and resulted skin reactions to hot regions viewed by Cherenkoscopy. Most likely, patients who undergo EBRT will be treated by 10 to 30 of fractions. If the superficial dose can be measured accurately in the early fractions, treatment plan for the following fractions of treatments could potentially be modified to avoid hot regions on the surface. With the ability to image treatment fields on the surface of the treatment region [Fig. 3(d) and Video 1] in real time, beam changes due to the motion of a dynamic wedge or multileaf collimators could be monitored to make sure treatments are delivered as planned.

In conclusion, *in vivo* Cherenkoscopy was acquired for the first time during EBRT in an animal undergoing standard radiation treatment for an oral tumor. This imaging is a novel approach for beam field monitoring and could be extended to radiation dose assessing in real time on the tissue surface during EBRT.

Acknowledgments

This work has been financially supported by Pilot Grant Funds from the Norris Cotton Cancer Center, as well as National Institutes of Health research grant R01CA109558.

References

1. P. A. Cherenkov, "The spectrum of visible radiation produced by fast electrons," *C. R. Acad. Sci.* **URSS20**, 651–655 (1938).
2. J. V. Jelley, "Cerenkov radiation and its applications," *Br. J. Appl. Phys.* **6**(7), 227–232 (1955).
3. R. Robertson et al., "Optical imaging of Cerenkov light generation from positron-emitting radiotracers," *Phys. Med. Biol.* **54**(16), N355–365 (2009).
4. A. E. Spinelli et al., "First human Cerenkography," *J. Biomed. Opt.* **18**(2), 020502 (2013).
5. J. Axelsson et al., "Cerenkov emission induced by external beam radiation stimulates molecular fluorescence," *Med. Phys.* **38**(7), 4127–4132 (2011).
6. A. K. Glaser et al., "Projection imaging of photon beams by the Cerenkov effect," *Med. Phys.* **40**(1), 012101 (2013).
7. A. K. Glaser et al., "Three-dimensional Cerenkov tomography of energy deposition from ionizing radiation beams," *Opt. Lett.* **38**(5), 634–636 (2013).
8. A. K. Glaser et al., "Projection imaging of photon beams using Cerenkov-excited fluorescence," *Phys. Med. Biol.* **58**(3), 601–619 (2013).
9. R. Zhang et al., "Oxygen tomography by Cerenkov-excited phosphorescence during external beam irradiation," *J. Biomed. Opt.* **18**(5), 050503 (2013).
10. R. Zhang et al., "Cerenkov radiation emission and excited luminescence (CREL) sensitivity during external beam radiation therapy: Monte Carlo and tissue oxygenation phantom studies," *Biomed. Opt. Express* **3**(10), 2381–2394 (2012).
11. R. Zhang et al., "Superficial dosimetry imaging based on Čerenkov emission for external beam radiotherapy with megavoltage x-ray beam," *Med. Phys.* **40**(10), 101914–101912 (2013).
12. R. Zhang et al., "Superficial dosimetry imaging of Cerenkov emission in electron beam radiotherapy of phantoms," *Phys. Med. Biol.* **58**(16), 5477–5493 (2013).
13. A. K. Glaser et al., "Time-gated Cherenkov emission spectroscopy from linear accelerator irradiation of tissue phantoms," *Opt. Lett.* **37**(7), 1193–1195 (2012).
14. L. Archambault, T. M. Briere, and S. Beddar, "Transient noise characterization and filtration in CCD cameras exposed to stray radiation from a medical linear accelerator," *Med. Phys.* **35**(10), 4342–4351 (2008).